



Thermal effects on the sedimentation behavior of elliptical particles

A. Xu, L. Shi, T.S. Zhao *

HKUST Energy Institute, Department of Mechanical and Aerospace Engineering, The Hong Kong University of Science and Technology, Hong Kong, China



ARTICLE INFO

Article history:

Received 19 March 2018

Received in revised form 13 May 2018

Accepted 15 May 2018

Keywords:

Particle flow

Lattice Boltzmann method

Heat transfer

Particle sedimentation

ABSTRACT

We investigate thermal effects on the sedimentation behavior of elliptical particles via particle-resolved direct numerical simulation. Two scenarios of fluid-particle heat transfer in an infinitely long channel are considered: one is a cold particle settling in a hot fluid, while the other is a hot particle settling in a cold fluid. Results show that when an elliptical particle sediment in a wide channel (i.e., the block ratio is large), in addition to the two sedimentation modes reported in the literature for the particle sediments in isothermal fluids, there exist another three modes arising from thermal effects: the tumbling mode, the anomalous rolling mode and the inclined mode. Specifically, for a cold particle settling in a hot fluid, we found the tumbling mode and inclined mode, while for a hot particle settling in a cold fluid, we found the anomalous rolling mode and inclined mode. The phase diagrams of the sedimentation modes as functions of Archimedes and Grashof numbers are given. Analyses of the relationship between particle Reynolds number and Grashof number indicates that the mode presented depends on the competition between channel wall confinement, combined forced and natural convection.

© 2018 Elsevier Ltd. All rights reserved.

1. Introduction

The motion of solid particles in a viscous fluid has wide applications in various engineering fields. For example, in suspension redox flow batteries, the size, shape, and composition of both active material particles and conductive material particles are intrinsically coupled parameters affecting the rheology and transport properties of suspension fluid [1]. In these scenario applications, both fluid inertia and viscosity are finite, the behavior of the fluids and solid particles are strongly coupled, thus particle motion shows rich physical phenomena. Among various parameters affecting particle motion, particle shape plays a critical role. During the past several decades, motion of spherical particles has drawn much attention due to the symmetry of particle shape. Recently, more researches focus on the motion of non-spherical particles to truly discover real-world particle transport processes.

For a two-dimensional (2D) elliptical particle or a three-dimensional (3D) ellipsoid particle sedimentation, eight distinct modes have been reported [2–5]: the horizontal mode, the horizontal II mode, the inclined mode, the inclined II mode, the vertical mode, the oscillatory mode, the anomalous rolling mode and the spiral mode. The horizontal mode refers to particle sediments horizontally with a constant velocity along the centerline of channel; while the horizontal II mode refers to particle sediments horizon-

tally with oscillating pattern. In the inclined mode, particle sediments with a constant velocity and a constant inclination to horizontal; while in the inclined II mode, inclined particle sediments with oscillating pattern. In the vertical mode, particle sediments vertically and it can be regarded as limitation of the inclined mode with inclination angle of 90°. The oscillatory mode means particle wiggles down channel, approaching two sides of the wall periodically and oscillating around channel centerline; while the anomalous rolling mode means falling particle rotates as if it was contacting and rolling up along one of channel walls. The spiral mode is unique in 3D ellipsoid particle settling, and it indicates particle spirals around channel centerline while the angle between the particle axis and channel centerline keeps constant. The above-mentioned modes are usually resulted from two effects: one is channel geometry effects, which is characterized by blockage ratio as channel width over particle axis length; the other is particle inertial effect, which is characterized by particle Reynolds number as a function of particle size and particle density. Specifically, Xia et al. [2] reported the horizontal mode and the horizontal II mode for a 2D elliptical particle sedimentation in a wide channel as particle density varies. In addition, they identified the oscillatory mode, the anomalous rolling mode (known as the tumbling mode in their paper), the vertical mode, the inclined mode and the horizontal model as blockage ratio varies when particle sediments in a narrow channel. By carrying out 3D simulation, Swaminathan et al. [3] found oscillatory and inclined modes for an ellipsoidal particle settling in a tube. To further verify whether the tumbling

* Corresponding author.

E-mail address: metzhao@ust.hk (T.S. Zhao).

mode, the vertical mode and the horizontal mode found in 2D simulations will occur in 3D simulation. Huang et al. [4] investigated the sedimentation of a prolate ellipsoid in both circular and square tubes, and they confirmed the spiral mode and the vertically inclined mode. Moreover, the phase diagram of flow regimes as functions of tube blockage ratio and Reynolds number are obtained. Later, same authors extended their investigation to study the sedimentation of an oblate ellipsoid [5].

The above studies focused on isothermal suspended particles where there is no thermal convection between suspended particles and surrounding fluids. However, thermal effects are not always negligible in studying particle suspension since heat transfer might significantly alter the particle kinematics. For example, Gan et al. [6] demonstrated that thermal convection can change sedimentation behavior of a 2D circular particle via two factors: one is the competition between natural and forced convection, and the other is wall effects. Feng and Michaelides [7] investigated heat transfer in particulate flows with a group of interacting circular particles and they showed how the local temperature field and buoyancy force affects both sedimentation process and energy transfer. Deen

et al. [8] investigated heat transfer of dense particulate systems in both stationary beds and fluidized beds. Hu and Guo [9] identified five competing mechanisms for lateral migration of a circular particle with thermal convection, namely the wall repulsion due to lubrication, the inertial lift related to shear slip, the lift due to particle rotation, the lift due to the curvature of the undisturbed velocity profile and the lift induced by thermal convection. However, it should be noted that in all previous studies involving particulate flows with heat transfer, only solid particles as the circular shape were considered to reduce the complexity of the problem.

With the knowledge presented in the above studies, one may ask what complex phenomena would arise for an elliptical particle sedimentation in non-isothermal fluids? To answer this question, in this work, we present a systemic investigation of thermal effects on elliptical particle sedimentation behavior. The rest of the paper is organized as follows: In Section 2, we first present the double-distribution multiple-relaxation-time lattice Boltzmann (LB) model for simulating fluid flows and heat transfer, followed by particle-resolved LB model for simulating particle suspension. In Section 3, the present LB model is evaluated by verifying sedimentation behavior of an elliptical particle in isothermal fluids, and a cold circular particle in a hot fluid. After that, numerical simulations are carried out to study a cold elliptical particle settling in a hot fluid and a hot elliptical particle settling in a cold fluid with various Archimedes and Grashof numbers.

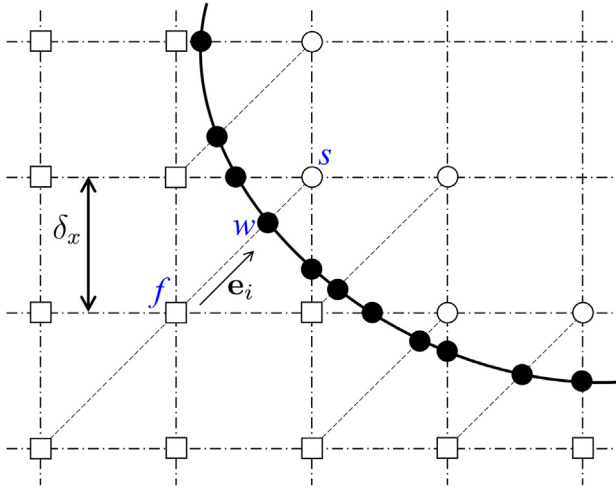


Fig. 1. Schematic drawing of curve wall boundary condition.

2. Numerical method

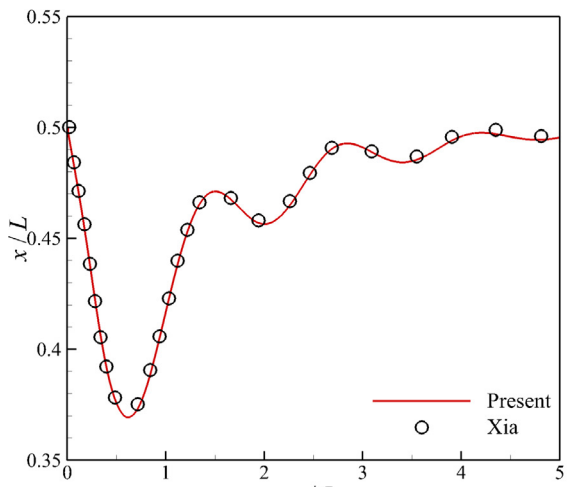
2.1. The double-distribution-function LB model for fluid flow and heat transfer

Incompressible fluid flows can be described by the Navier-Stokes equations; while buoyancy effect caused by temperature variation can be approximated by the Boussinesq approximation [10–13]. Then, the governing equations of fluid flow and heat transfer can be written as

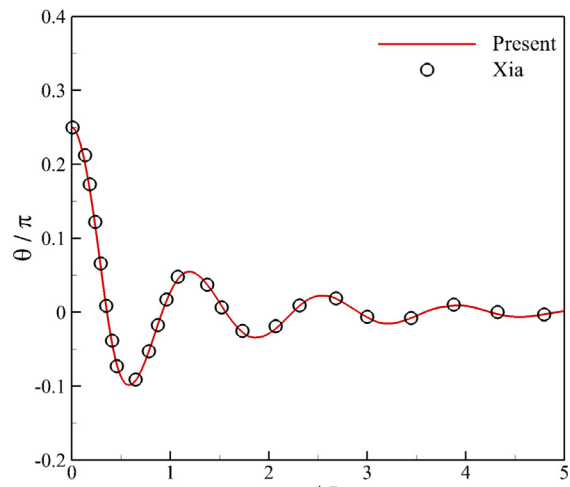
$$\nabla \cdot \mathbf{u} = 0 \quad (1a)$$

$$\frac{\partial \mathbf{u}}{\partial t} + \mathbf{u} \cdot \nabla \mathbf{u} = -\frac{1}{\rho_0} \nabla p + \nu \nabla^2 \mathbf{u} + g \beta_T (T - T_0) \hat{\mathbf{y}} \quad (1b)$$

$$\frac{\partial T}{\partial t} + \mathbf{u} \cdot \nabla T = \kappa \nabla^2 T \quad (1c)$$



(a) Trajectories



(b) Orientations

Fig. 2. Time histories of the elliptical particle settling in a wide channel ($\beta = 4$).

where \mathbf{u} is the fluid velocity, ρ is the fluid density, p is the pressure, and ν is the kinematic viscosity. T is the temperature, β_T is the thermal expansion coefficient, and κ is the thermal diffusivity. g is the gravity value, and $\hat{\mathbf{y}}$ is unit vector in the vertical direction. ρ_0 and T_0 are reference density and temperature, respectively. With the scaling $\mathbf{x}/L_0 \rightarrow \mathbf{x}^*, t/(\frac{L_0}{\kappa}) \rightarrow t^*, \mathbf{u}/(\frac{\kappa}{L_0}) \rightarrow \mathbf{u}^*, p/(\frac{\rho_0 \kappa^2}{L_0^2}) \rightarrow p^*, (T - T_0)/\Delta T \rightarrow T^*$, then Eqs. (1a)–(1c) can be rewritten in dimensionless form as

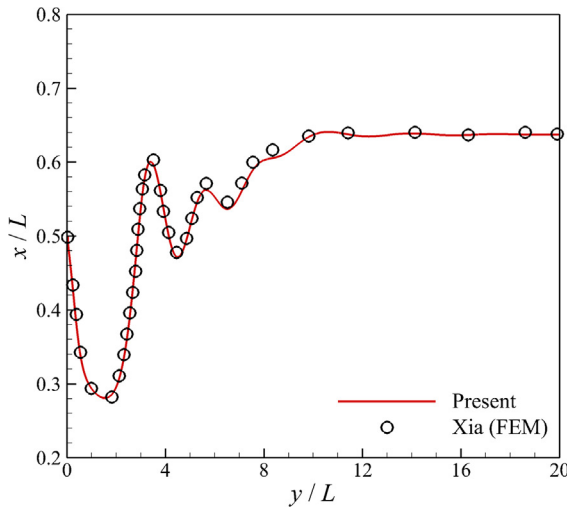
$$\nabla \cdot \mathbf{u}^* = 0 \quad (2a)$$

$$\frac{\partial \mathbf{u}^*}{\partial t^*} + \mathbf{u}^* \cdot \nabla \mathbf{u}^* = -\nabla p^* + Pr \nabla^2 \mathbf{u}^* + Gr Pr^2 T^* \hat{\mathbf{y}} \quad (2b)$$

$$\frac{\partial T^*}{\partial t^*} + \mathbf{u}^* \cdot \nabla T^* = \nabla^2 T^* \quad (2c)$$

where the Prandtl number is $Pr = \nu/\kappa$, and the Grashof number is $Gr = g\beta_T \Delta T L_0^3 / \nu^2$.

To solve the above equations, the double-distribution-function LB model can be adopted, namely, two LB equations are solved to simulate flow field and temperature field, respectively [14–16].



(a) Trajectories

The evolution equations of density distribution function f_i and temperature distribution function g_i can be written as

$$f_i(\mathbf{x} + \mathbf{e}_i \delta_t, t + \delta_t) - f_i(\mathbf{x}, t) = -(\mathbf{M}^{-1} \mathbf{S})_{ij} [\mathbf{m}_j(\mathbf{x}, t) - \mathbf{m}_j^{(eq)}(\mathbf{x}, t)] + \delta_t F_i \quad (3a)$$

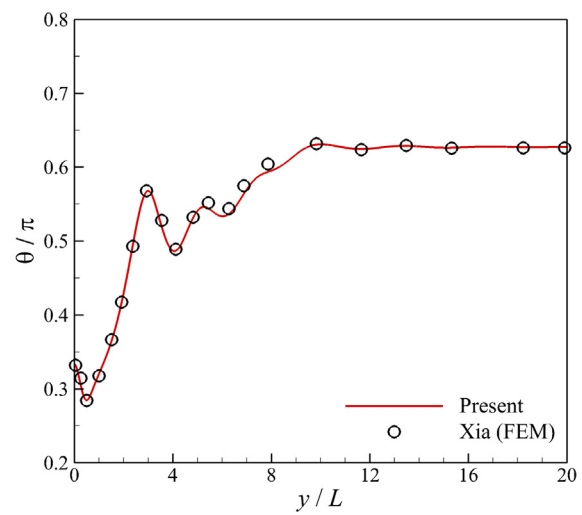
$$g_i(\mathbf{x} + \mathbf{e}_i \delta_t, t + \delta_t) - g_i(\mathbf{x}, t) = -(\mathbf{N}^{-1} \mathbf{Q})_{ij} [\mathbf{n}_j(\mathbf{x}, t) - \mathbf{n}_j^{(eq)}(\mathbf{x}, t)] \quad (3b)$$

where t is the time, δ_t is the time step, \mathbf{x} is fluid parcel position, and \mathbf{e}_i is discrete velocity along the i th direction. $\mathbf{F} = \mathbf{M}^{-1} (\mathbf{I} - \frac{s}{2}) \tilde{\mathbf{M}}$ is the forcing term in velocity space, where $\mathbf{M}\tilde{\mathbf{F}}$ is given by [17,18].

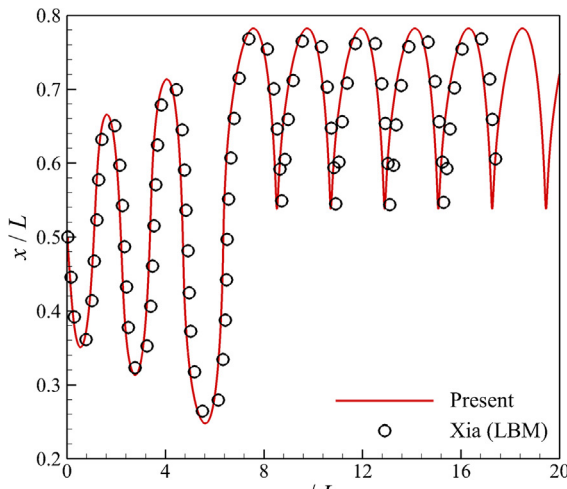
$$\mathbf{M}\tilde{\mathbf{F}} = [0, 6\mathbf{u} \cdot \mathbf{F}, -6\mathbf{u} \cdot \mathbf{F}, F_x, -F_x, F_y, -F_y, 2(u_x F_x - u_y F_y), (u_x F_y + u_y F_x)]^T \quad (4)$$

Here, the external body force is $\mathbf{F} = g\beta_T(T - T_0)\hat{\mathbf{y}}$. The equilibrium moments $\mathbf{m}^{(eq)}$ is given by

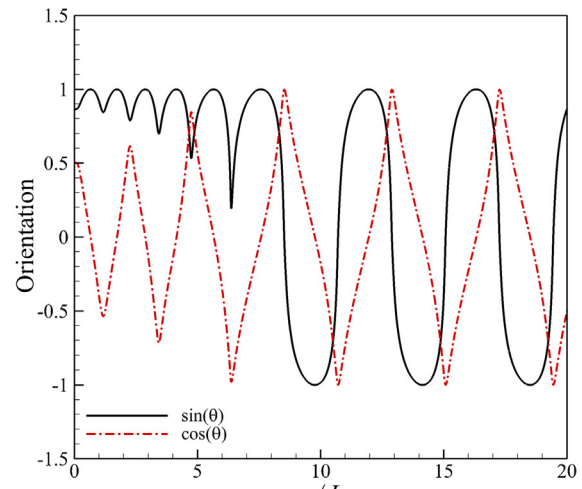
$$\mathbf{m}^{(eq)} = \left[\rho, -2\rho + \frac{3}{\rho}(j_x^2 + j_y^2), \rho - \frac{3}{\rho}(j_x^2 + j_y^2), j_x, -j_x, j_y, -j_y, \frac{1}{\rho}(j_x^2 - j_y^2), \frac{1}{\rho}j_x j_y \right]^T \quad (5)$$



(b) Orientations

Fig. 3. Time histories of the elliptical particle settling in a narrow channel ($\beta = 1.69$).

(a) Trajectories



(b) Orientations

Fig. 4. Time histories of the elliptical particle settling in a narrow channel ($\beta = 1.23$).

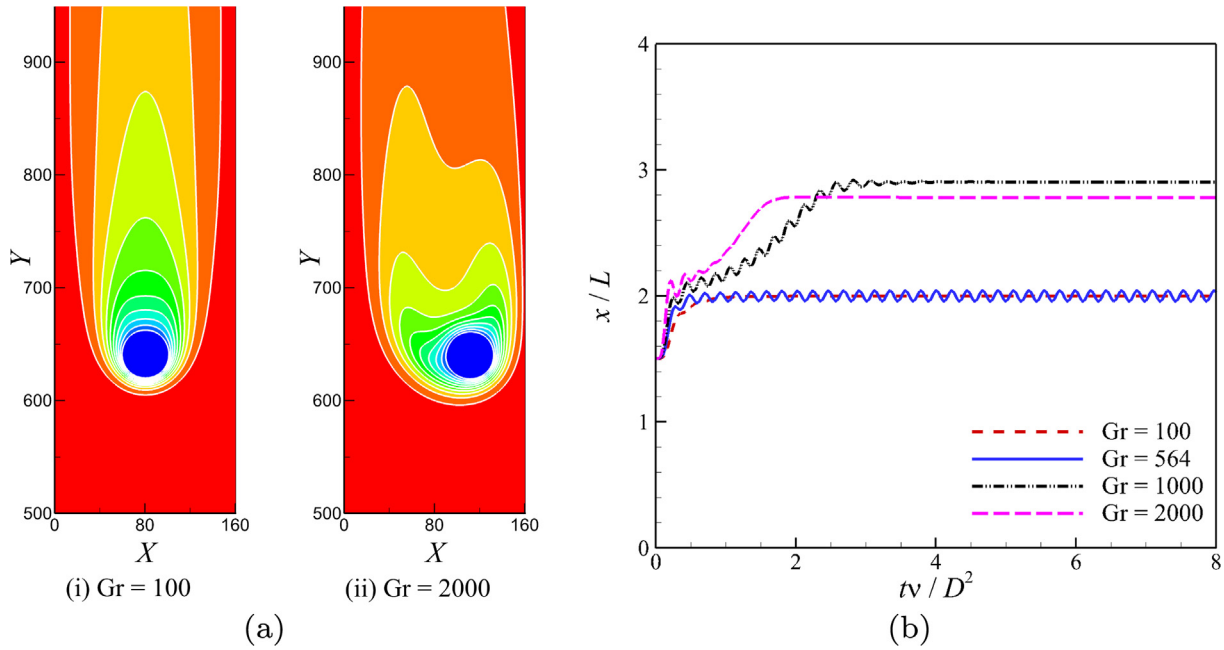


Fig. 5. (a) Isotherms of circular particle sedimentation; (b) time history of the horizontal position of the particle.

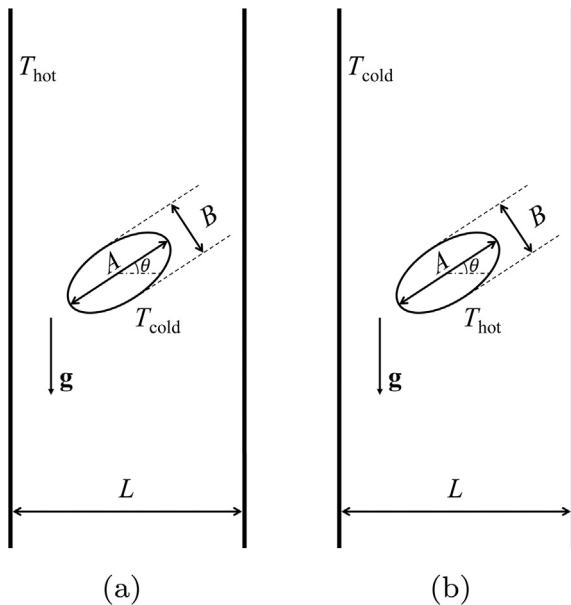


Fig. 6. Schematic drawing of (a) a cold elliptical particle settling in a hot fluid; (b) a hot elliptical particle settling in a cold fluid.

and the relaxation matrix \mathbf{S} is given by $\mathbf{S} = \text{diag}(s_p, s_e, s_\epsilon, s_j, s_q, s_v, s_y)$, where the relaxation parameters are $s_p = s_j = 0$, $s_e = s_\epsilon = s_v = 1/\tau_f$, $s_q = 8(2\tau_f - 1)/(8\tau_f - 1)$. τ_f is determined by the kinematic viscosity of the fluids as $\tau_f = 3v + 0.5$. The transformation matrix \mathbf{M} is given by Lallemand and Luo [19]. The density ρ and velocity \mathbf{u} are calculated as $\rho = \sum_{i=0}^8 f_i$, $\mathbf{u} = \frac{1}{\rho} \left(\sum_{i=0}^8 \mathbf{e}_i f_i + \frac{1}{2} \mathbf{F} \right)$. The equilibrium moments $\mathbf{n}^{(\text{eq})}$ is given by

$$\mathbf{n}^{(\text{eq})} = [T, uT, vT, a_T T, 0]^T \quad (6)$$

where a_T is a constant determined by the thermal diffusivity of the fluids as $a_T = 20\sqrt{3}\kappa - 4$. The relaxation matrix \mathbf{Q} is given by $\mathbf{Q} = \text{diag}(0, q_T, q_T, q_e, q_v)$, where the relaxation parameters are

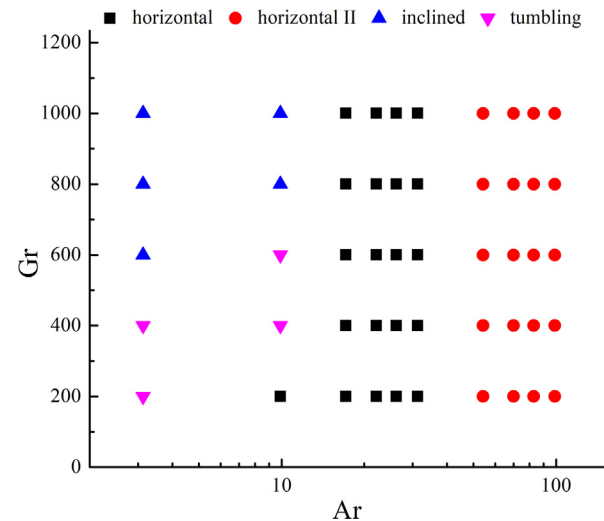


Fig. 7. Phase diagram of a cold elliptical particle settling in a hot fluid within a wide channel.

$q_T = 3 - \sqrt{3}$ and $q_e = q_v = 4\sqrt{3} - 6$. The transformation matrix \mathbf{N} is given by Wang et al. [20]. The temperature T is calculated as $T = \sum_{i=0}^4 g_i$.

2.2. Translation and rotation of the solid particle

The solid particle is considered as rigid body and the kinematics of the particle include translational and rotational motion [21–24]. The translational motion of the solid particle is determined by Newton's second law as

$$M_p \frac{d\mathbf{U}_c(t)}{dt} = \mathbf{F}_p(t) \quad (7)$$

where M_p is the mass of the particle, \mathbf{U}_c is the velocity of the particle center and \mathbf{F}_p is the total force exerted on the solid particle. The

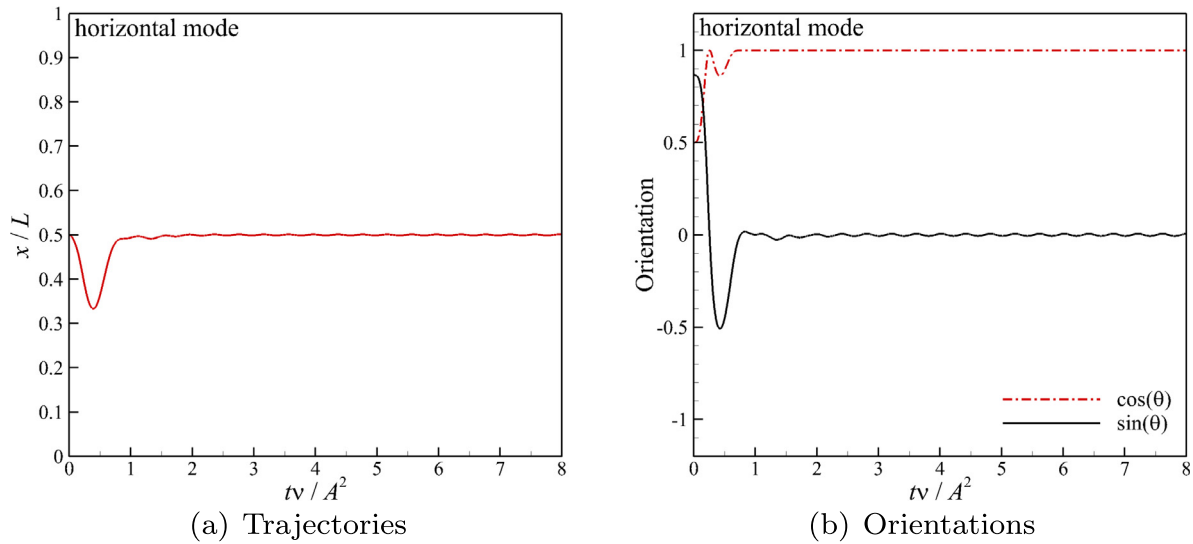
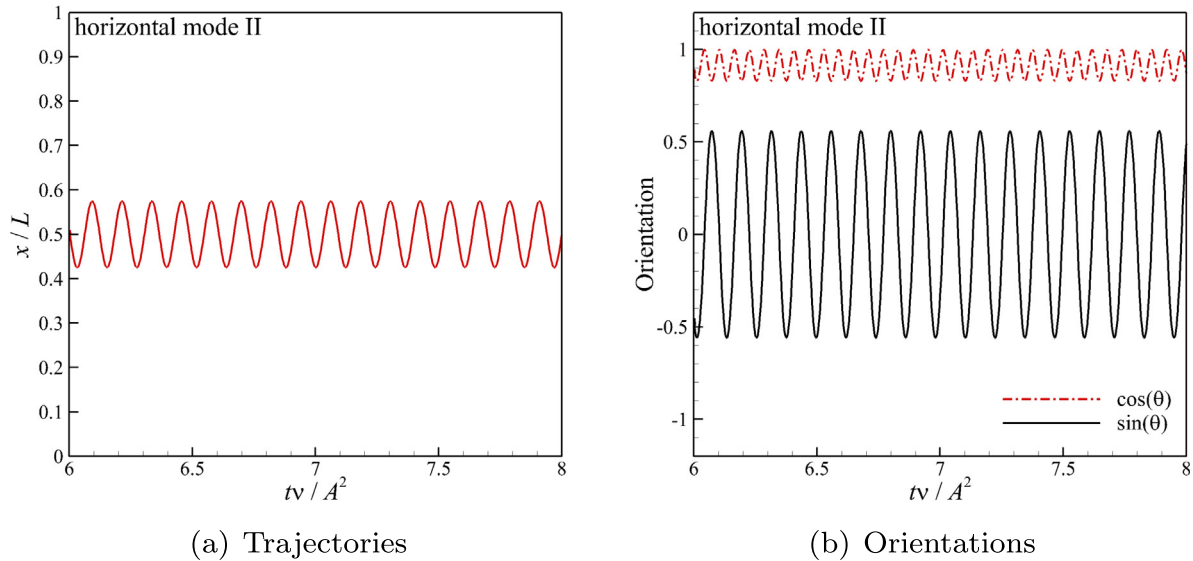
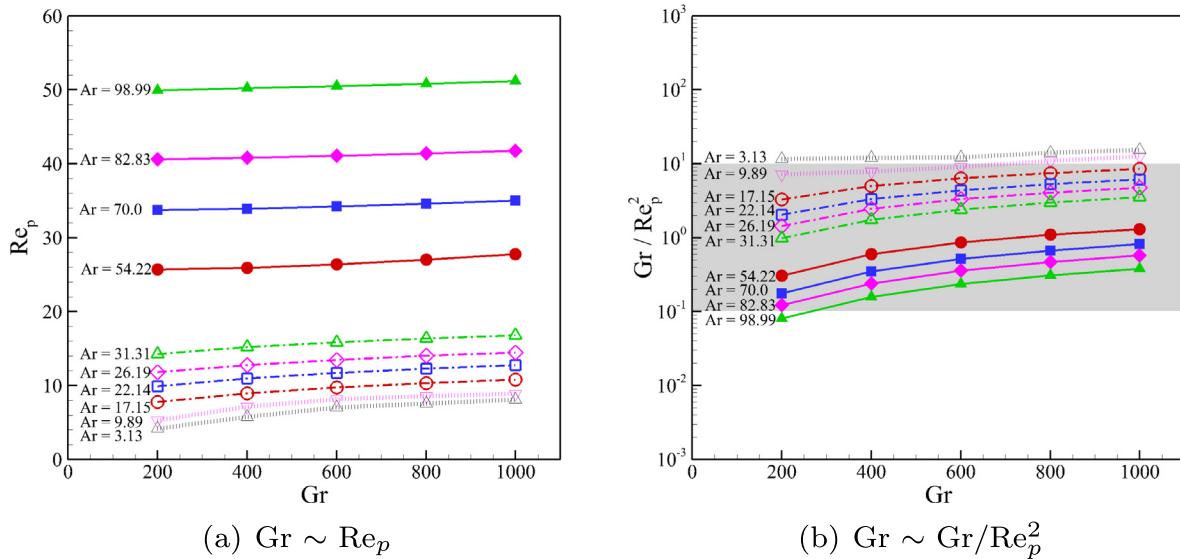
Fig. 8. Time histories of the elliptical particle settling ($Ar = 17.15$, $Gr = 600$).Fig. 9. Time histories of the elliptical particle settling ($Ar = 82.83$, $Gr = 600$).

Fig. 10. The particle Reynolds number as a function of Grashof number (for a cold elliptical particle settling in a hot fluid).

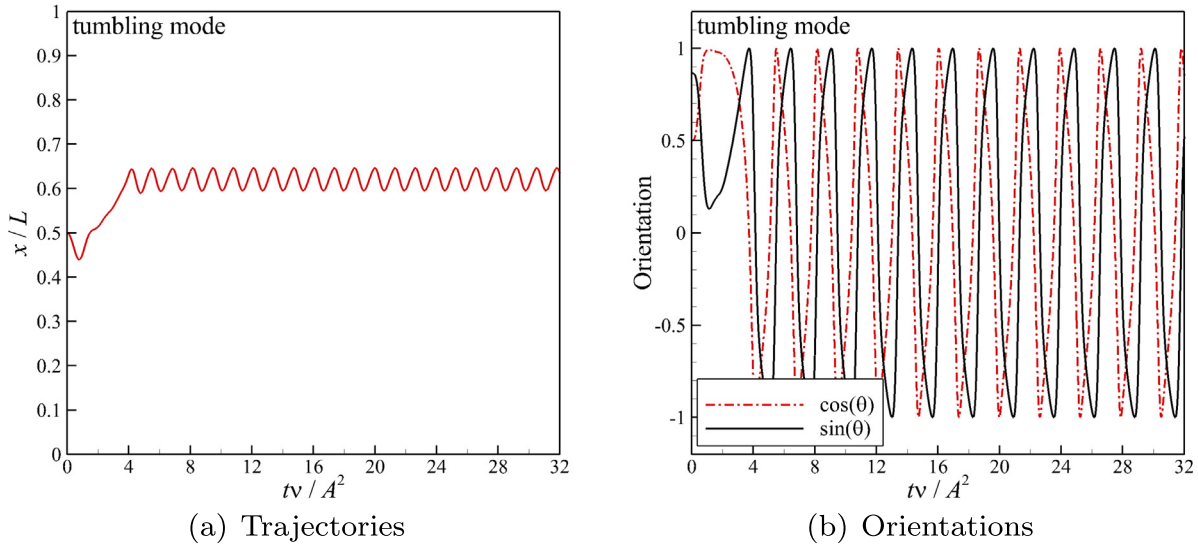


Fig. 11. Time histories of the elliptical particle settling ($Ar = 3.13$, $Gr = 200$).

rotational motion of the solid particle is determined by Euler's second law as

$$\mathbf{I}_p \cdot \frac{d\boldsymbol{\Omega}(t)}{dt} + \boldsymbol{\Omega}(t) \times [\mathbf{I}_p \cdot \boldsymbol{\Omega}(t)] = \mathbf{T}_p(t) \quad (8)$$

where \mathbf{I}_p is inertial tensor of the particle, $\boldsymbol{\Omega}$ is angular velocity and \mathbf{T}_p is torque exerted on the solid particle.

2.3. Fluid-solid boundary interaction

At the particle's surface, the interpolated bounce-back scheme for curved wall boundaries is adopted to guarantee no-slip boundary condition [25–30]. Define the parameter $q = |\mathbf{x}_f - \mathbf{x}_w| / |\mathbf{x}_f - \mathbf{x}_s|$ to describe the fraction of fluid region in a grid spacing intersected by solid surface, where \mathbf{x}_f is fluid node near the boundary, \mathbf{x}_s is solid node near the boundary and \mathbf{x}_w is the wall of fluid-solid interface. Based on the relative location of \mathbf{x}_w between \mathbf{x}_f and \mathbf{x}_s (as shown in Fig. 1), the interpolation scheme of density distribution function is given as [26]: for $q \leq 0.5$

$$f_i(\mathbf{x}_f, t) = q(2q+1)f_i(\mathbf{x}_f + \mathbf{e}_i\delta_t, t) + (1-4q^2)f_i(\mathbf{x}_f, t) - q(1-2q)f_i(\mathbf{x}_f - \mathbf{e}_i\delta_t, t) + 2\omega_i\rho_0 \frac{\mathbf{e}_i \cdot \mathbf{u}_w}{C_s^2} \quad (9)$$

for $q \geq 0.5$

$$f_i(\mathbf{x}_f, t) = \frac{1}{q(2q+1)} f_i(\mathbf{x}_f + \mathbf{e}_i \delta_t, t) + \frac{2q-1}{q} f_{\bar{i}}(\mathbf{x}_f - \mathbf{e}_i \delta_t, t) - \frac{2q-1}{2q+1} f_i(\mathbf{x}_f - 2\mathbf{e}_i \delta_t, t) + \frac{1}{q(2q+1)} 2\omega_i \rho_0 \frac{\mathbf{e}_i \cdot \mathbf{u}_w}{C_w^2} \quad (10)$$

where f_i is the distribution function associated with the velocity $\mathbf{e}_i = -\mathbf{e}_j$.

We assume the fluids and particle temperatures equal to a constant T_w at the surface of the particle. Then the bounce-back scheme for the temperature distribution function g_i at curved wall boundaries is given as [31, 32]:

$$\begin{aligned} \bar{g}_i(\mathbf{x}_f, t + \delta_t) = & \left[c_{d1} g_i^+(\mathbf{x}_f, t) + c_{d2} g_i^+(\mathbf{x}_f + \mathbf{e}_i \delta_t, t) + c_{d3} g_i^+(\mathbf{x}_f, t) \right] \\ & + c_{d4} (2\omega_i T_w) \end{aligned} \quad (11)$$

where g_i^- is the distribution function associated with the velocity $\mathbf{e}_i = -\mathbf{e}_i^+$, and g_i^+ is the post-collision distribution function. The coefficients c_{d1-4} are given as

$$c_{d1} = -1, \quad c_{d2} = \frac{2q-1}{2q+1}, \quad c_{d3} = \frac{2q-1}{2q+1}, \quad c_{d4} = \frac{2}{2q+1} \quad (12)$$

To calculate the force and torque exerted by the fluid on the solid particle, the momentum-exchange method is adopted, namely, hydrodynamic force acting on the solid surface is obtained by summing up the local momentum exchange of the fluid parcels during the bounce back process at fluid-solid interface over boundary links [33]. To restore the Galilean invariance, the modified momentum-exchange method proposed by Wen et al. [34] is adopted. Then, the total force is calculated as

$$\mathbf{F} = \sum_{\mathbf{x}_f} \sum_{i \in I_f} [f_i^+(\mathbf{x}_f, t)(\mathbf{e}_i - \mathbf{u}_w) - f_i(\mathbf{x}_f, t + \delta_t)(\mathbf{e}_i - \mathbf{u}_w)] \quad (13)$$

and the total torque is calculated as

$$\mathbf{T} = \sum_{\mathbf{x}_f} \sum_{i_{bl}} (\mathbf{x}_w - \mathbf{x}_c) \times [f_i^+(\mathbf{x}_f, t)(\mathbf{e}_i - \mathbf{u}_w) - f_i^-(\mathbf{x}_f, t + \delta_t)(\mathbf{e}_i - \mathbf{u}_w)] \quad (14)$$

To prevent overlap between the particle and the wall when their distance is small, artificial repulsive force model should be adopted. Here, we choose the spring force model proposed by Feng and Michaelides [35], which is written as

$$\mathbf{F}_{\text{repulsive}} = \begin{cases} 0 & \text{if } |\mathbf{x}_s| > \xi, \\ \frac{C}{\epsilon_w} \left(\frac{|\mathbf{x}_s| - \xi}{\xi} \right)^2 \frac{\mathbf{x}_s}{|\mathbf{x}_s|} & \text{if } |\mathbf{x}_s| \leq \xi. \end{cases} \quad (15)$$

Here, ε_w represents the stiffness parameter and ξ represents the threshold distance. C is the force scale, \mathbf{x}_s denotes the vector with smallest norm value that points from the wall to the particle.

3. Validation

3.1. Validation I: Sedimentation of an elliptical particle in isothermal fluids

We consider an elliptical particle settling in an infinite long channel filled with isothermal fluids. The particle is released along the vertical centerline of the channel with an initial angle θ_0 between the particle major axis and the horizontal direction. In the simulations, the lengths of major axis A and minor axis B of the elliptical particle are $A = 0.1$ cm and $B = 0.05$ cm, respectively. The density and dynamic viscosity of the liquid are $\rho_f = 1$ g/cm³ and $\mu = 0.01$ g/(cm · s), respectively. The density of the solid

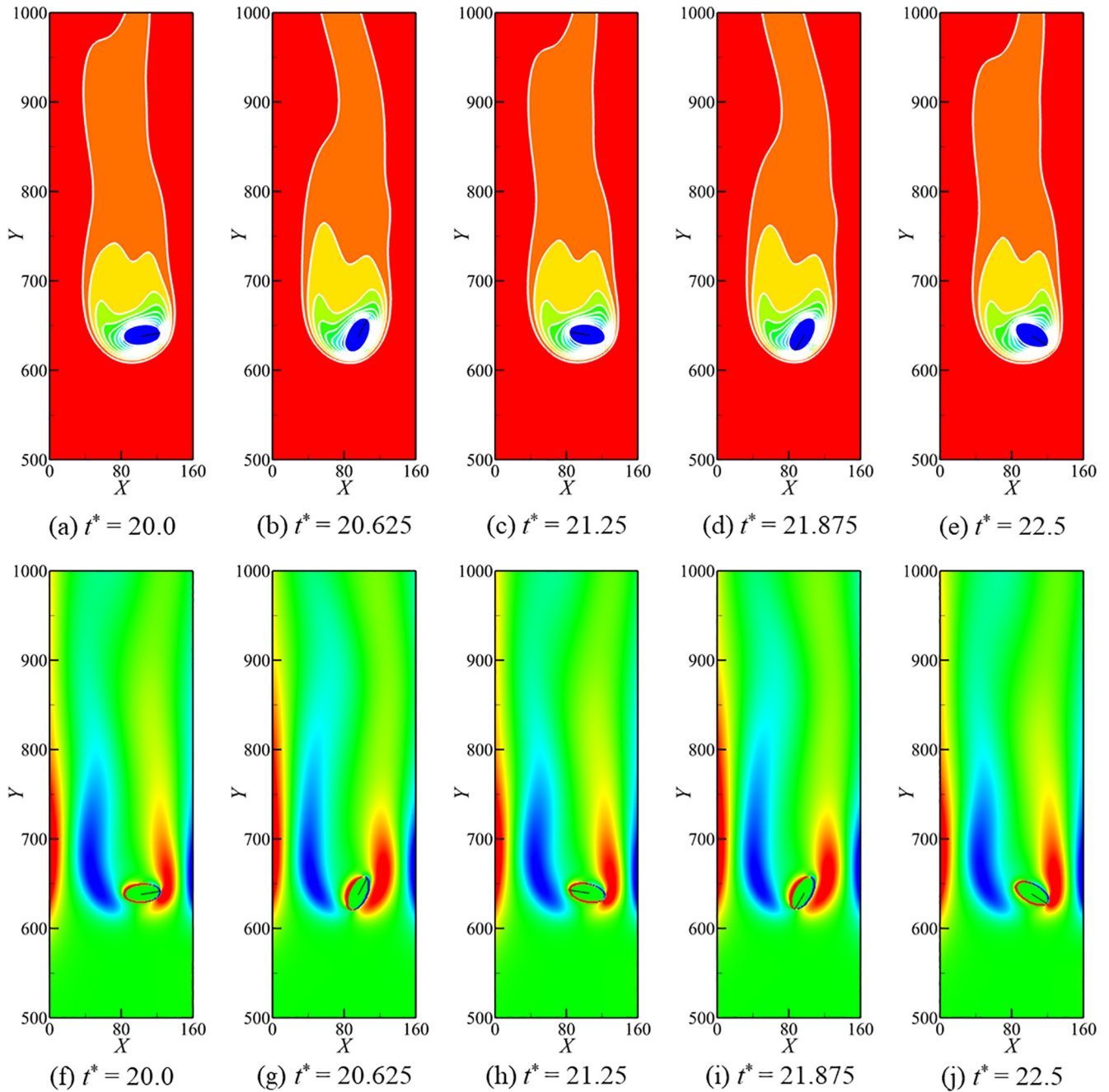


Fig. 12. Temperature and vorticity contours of the cold elliptical particle settling in a wide channel ($Ar = 3.13$, $Gr = 200$).

particle is $\rho_s = 1.1 \text{ g/cm}^3$. Zero velocity is applied at the inlet; the normal derivative of velocity is zero at the outlet. To mimicking an infinite long channel while saving the computational cost and minimizing the end effects, the moving computational domain technique [36] is adopted so that the vertical position of the particle is kept at approximately half of the computational domain.

Fig. 2 shows the particle trajectories and particle orientations during the sedimentation in a wide channel with blockage ratio $\beta = L/A = 4$, where L is the channel width. Grid independence and time-step independence studies are performed to determine that mesh size of 120×960 and time step with $\tau_f = 0.5375$ is small enough to get accurate results. Data reported by Xia et al. [2] is also provided as comparison. To further investigate effects of channel walls on the sedimentation behavior of the particle,

the blockage ratio is decreased to $\beta = 1.69$ and $\beta = 1.23$. Results are shown in Figs. 3 and 4, respectively. We can see that the present results agree well with Xia et al.'s results [2], and the reported inclined mode (as shown in Fig. 3) and tumbling mode (as shown in Fig. 4) are reproduced.

3.2. Validation II: Sedimentation of a cold circular particle in a hot fluid

We consider a cold circular particle settling in an infinitely long channel filled with a hot fluid. The vertical walls of the channel are maintained at a constant high temperature, while the surface of the particle is maintained at a low temperature. In the simulations, the particle is released off the vertical channel centerline by half of the particle diameter (D). The density ratio between the solid

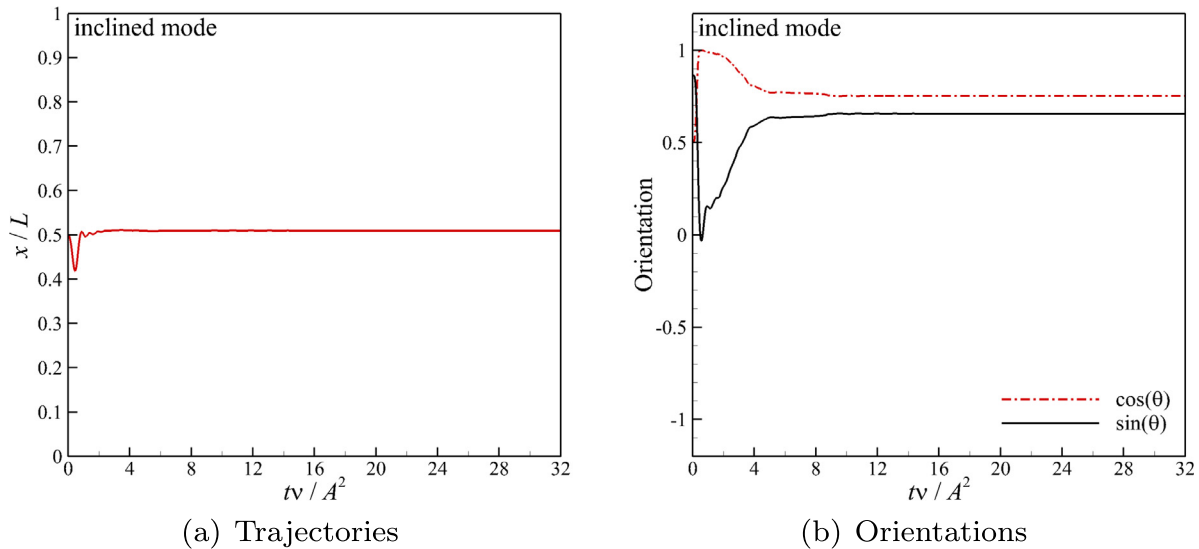


Fig. 13. Time histories of the elliptical particle settling ($Ar = 3.13$, $Gr = 600$).

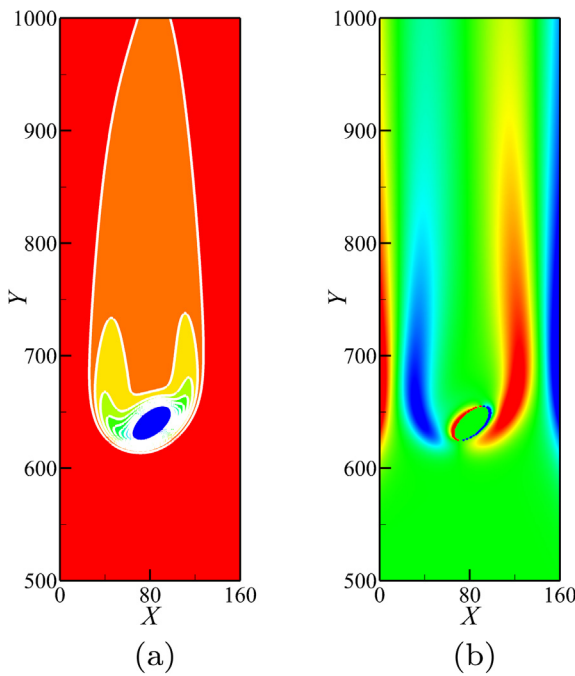


Fig. 14. Contours of (a) temperature and (b) vorticity of the elliptical particle settling ($Ar = 3.13$, $Gr = 600$).

particle and the fluid is $\rho_r = \rho_s/\rho_f = 1.00232$. The width of the channel is four times the diameter of the circular particle. The Prandtl number is fixed as $Pr = 0.7$. Grid independence and time-step independence studies are performed to determine that mesh size of 160×1280 and time step with $\tau_f = 0.5015$ is small enough to get accurate results.

Fig. 5 demonstrates that when the viscous force is dominated (e.g., at $Gr = 100$), the particle will eventually sediment along the vertical centerline of the channel, and the temperature field around the particle exhibits symmetry pattern; when the buoyancy force is dominated (e.g., at $Gr = 2000$), the particle will eventually sediment off the vertical channel centerline, and the offset distance is influenced by the Gr number. The equilibrium positions of the settling particle, which can be determined from Fig. 5b, also agree

with that reported by Feng and Michaelides [7], Yu et al. [37], Kang and Hassan [38].

4. Results and discussion

We now investigate the sedimentation behavior of a cold elliptical particle settling in an infinitely long channel filled with a hot fluid and a hot elliptical particle settling in an infinitely long channel filled with a cold fluid, as the schematic drawing shown in Fig. 6. The length of the elliptical particle's major axis is A , and the density of the particle is ρ_s ; the width of the channel is L . The density, viscosity, thermal expansion coefficient and thermal diffusivity of the fluids is ρ_f , v , β_T and κ , respectively. The gravity acceleration is denoted by g . The temperature difference between the bulk fluids and particle's surface is denoted by ΔT . The non-dimensional parameters in this problem include the blockage ratio $\beta = L/A$, the density ratio $\Delta\rho/\rho_f = (\rho_s - \rho_f)/\rho_f$, the Prandtl number $Pr = v/\kappa$, the Archimedes number $Ar = \sqrt{\frac{\Delta\rho}{\rho_f} \frac{gA^3}{v^2}}$ and the Grashof number $Gr = \sqrt{\frac{g\beta_T \Delta T A^3}{v^2}}$. In this study, we set the Prandtl number as $Pr = 7$; we fix $\frac{gA^3}{v^2}$, namely the density ratio and the Archimedes number are not independent; we choose the blockage ratio $\beta = 4$, namely particle sediments in a wide channel. Thus, remaining non-dimensional parameters under investigation will be (Ar, Gr) . We assume the solid particles have high thermal conductivity such that the temperature of the particle is regarded as constant. Grid independence and time-step independence studies are performed to determine that mesh size of 160×1280 and time step with $\tau_f = 0.503$ is small enough to get accurate results. In the following, we will discuss the sedimentation behaviors of both cold elliptical particle and hot elliptical particle.

4.1. A cold elliptical particle settling in an infinitely long channel filled with a hot fluid

We first consider the sedimentation behavior of a cold elliptical particle in an infinitely long channel filled with hot fluids. The sedimentation mode distribution on the (Ar, Gr) -plane is shown in Fig. 7. We can observe four distinct sedimentation modes: the horizontal mode, the horizontal II mode, the inclined mode and the

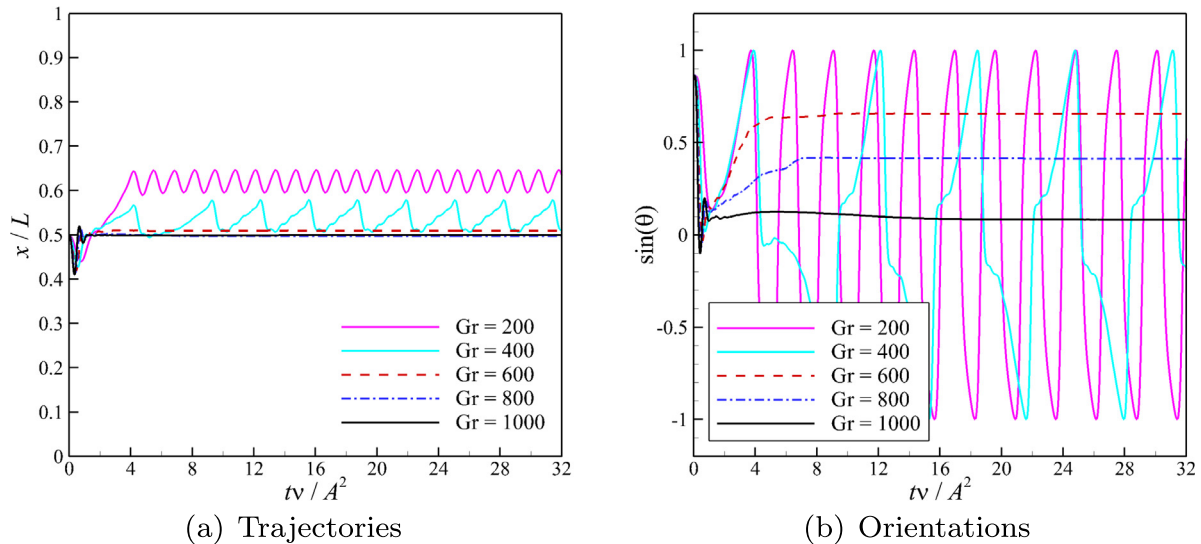


Fig. 15. Time histories of the elliptical particle settling in a wide channel ($Ar = 3.13$).

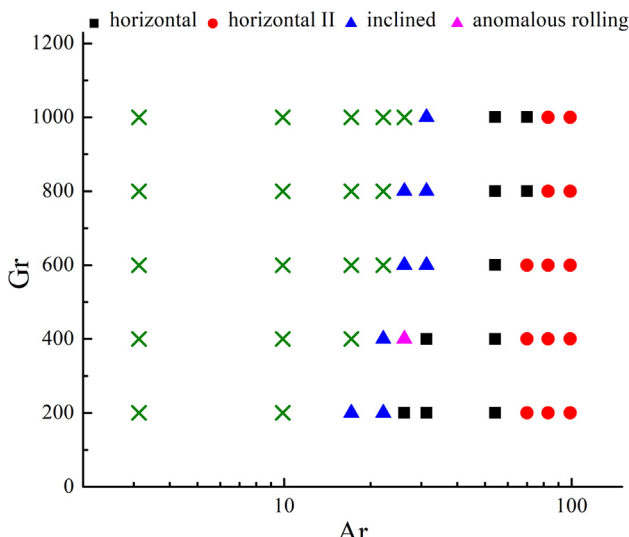


Fig. 16. Phase diagram of a hot elliptical particle settling in a cold fluid within a wide channel (the green cross represents that the hot particle is lifted up in the cold fluid due to buoyancy force). (For interpretation of the references to colour in this figure legend, the reader is referred to the web version of this article.)

tumbling mode. Compared to the sedimentation modes reported by Xia et al. [2] for an isothermal elliptical particle sediment within a wide channel, two new sedimentation modes are found arising from thermal effects. In the following, we will discuss these modes in detail.

From the phase diagram, it is observed that when $10 < Ar < 50$, the settling particle exhibits the horizontal mode; when $50 < Ar < 100$, the settling particle exhibits the horizontal II mode. These findings are consistent with that of isothermal particle sedimentations [2]. Typical trajectories and orientations of the horizontal mode and horizontal II mode are shown in Figs. 8 and 9, respectively. In the horizontal mode, the particle sediments horizontally along the centerline of the channel, namely the position of the particle center keeps at around $x/L = 0.5$, and the angle between particle major axis and horizontal direction keeps around $\theta = 0$. In the horizontal II mode, the particle sediments with oscillating pattern for both the horizontal position (around $x/L = 0.5$ as shown in

Fig. 9a) and incline angle (around $\theta = 0$ as shown in Fig. 9b). We further analyze the correlation of particle Reynolds number ($Re_p = uA/v$, where u represents the terminal particle settling velocity) as a function of the Grashof number when particle sediments in the horizontal mode and horizontal II mode. As shown in Fig. 10a, at the same Grashof number, the particle Reynolds number increases with the increases of Archimedes number; at the same Archimedes number, the particle Reynolds number increases slightly with the increases of Grashof number. This can be understood as the influence of both forced convection and natural convection on the particle motion, and it is further demonstrated in Fig. 10b that when the particle sediments in horizontal and horizontal II modes $Gr/Re_p^2 \approx 1$. For the cold particle settling in hot fluids, the downward temperature-induced buoyancy force is in the same direction with the gravity force, then the increases of Grashof number, namely the increases of natural convection, will augment the particle sedimentation.

When $1 < Ar < 10$, two new sedimentation modes are found arising from thermal effects: the tumbling mode and the inclined mode. Typical trajectories and orientations of the tumbling mode are shown in Fig. 11. The particle trajectory oscillates slightly off-sets the channel centerline (near the right wall), and the angle between particle major axis and horizontal direction changes periodically from 0 to 2π with counterclockwise rotation. The temperature contours and vorticity contours of the settling particle during a rotation period is further visualized in Fig. 12a-e and f-j, respectively.

Fig. 13 shows typical trajectories and orientations of the particle when it sediments in the inclined mode. We can see the particle sediments with a constant velocity and a constant inclination to horizontal. It should be noted that the inclined mode reported here is the result of competition of natural convection and forced convection; while the inclined mode observed by Xia et al. [2] is the result of channel wall confinement as the blockage ratio is small ($\beta < 2$). We can see from Fig. 13a that the particle center sediments along the channel centerline demonstrating the inclined mode reported here is not influenced by the wall effects; we can also see from Fig. 10b that natural convection is more prominent for the settling particle. Fig. 14 further visualized the temperature contours and vorticity when the particle sediments in the inclined mode.

We now discuss the evolution of particle settling modes from the tumbling mode to inclined mode at the same Archimedes num-

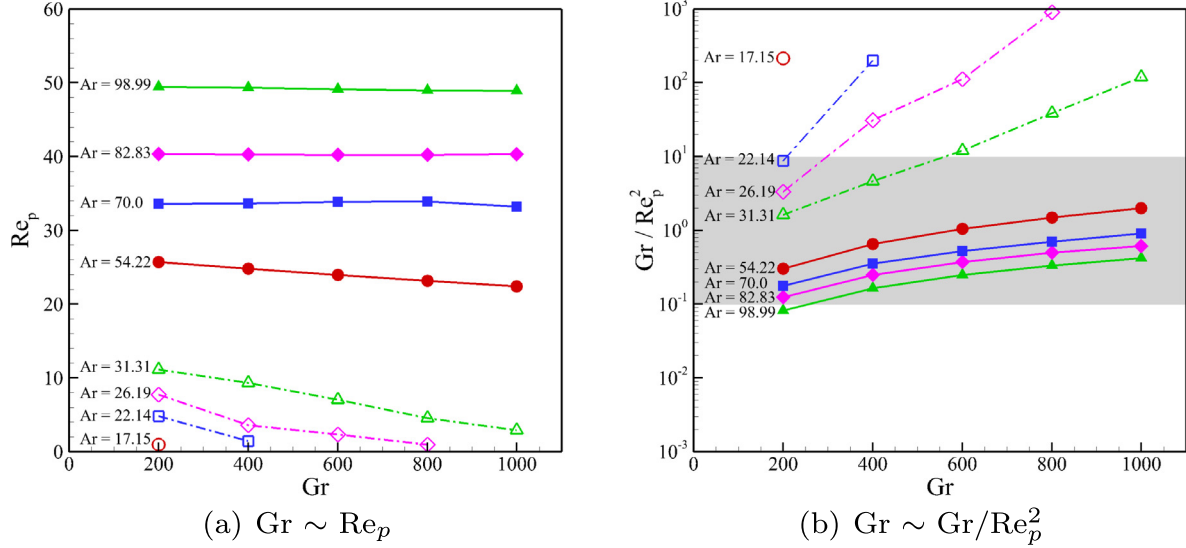


Fig. 17. The particle Reynolds number as a function of Grashof number (for a hot elliptical particle settling in a cold fluid).

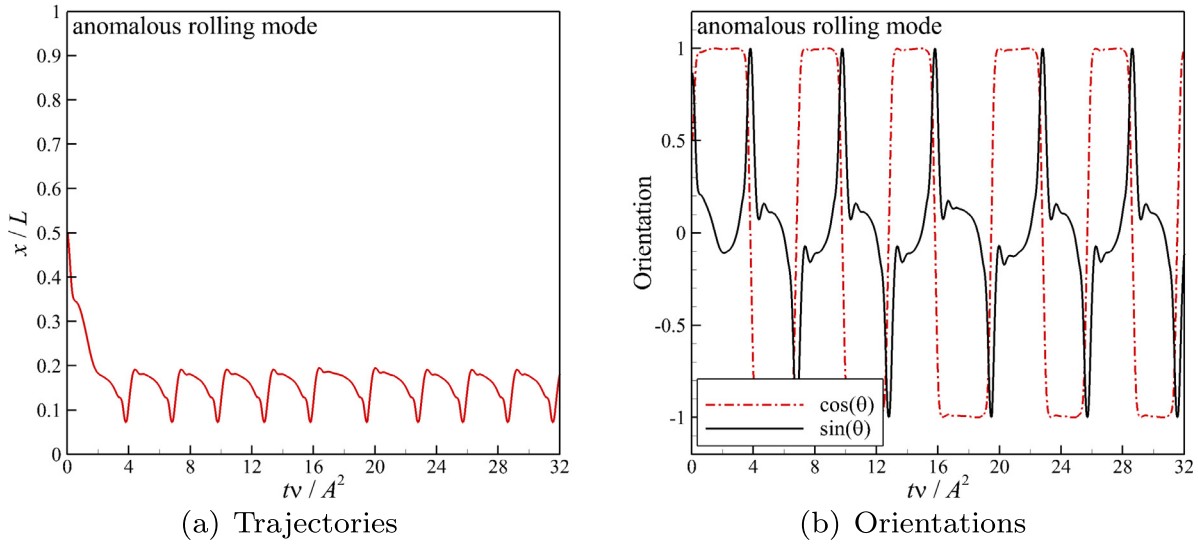


Fig. 18. Time histories of the elliptical particle settling in a wide channel ($Ar = 26.19$, $Gr = 400$).

ber. In the tumbling mode, with the increase of Grashof number, the rotation period of the particle is increased and the offset of the particle from the channel centerline is decreased (as shown in Fig. 15). Further increasing of Grashof number leads to the tumbling particle enters the inclined mode, where the angle between particle major axis and horizontal direction keeps constant and the particle's rotation period can be regarded as infinite. In the inclined mode, with the increase of Grashof number, the angle between particle major axis and horizontal direction decreases. These modes transition can be understood as the influence of increased natural convection on the particle sedimentation. For a cold particle settling in a hot fluid, the cold fluid layer next to the particle moving downward counters the upward external flow, and this will cause vortex shedding and oscillation of the wake. Larger Grashof number will argument natural convection which resulted in competitive natural and forced convection, and further leads to symmetric vortex and steady-state settling.

4.2. A hot elliptical particle settling in an infinitely long channel filled with a cold fluid

We then consider the sedimentation behavior of a hot elliptical particle in an infinitely long channel filled with a cold fluid. The sedimentation mode distribution on the (Ar , Gr)-plane is shown in Fig. 16. We can observe four distinct sedimentation modes: the horizontal mode, the horizontal II mode, the inclined mode and the anomalous rolling mode. In addition, we found that the elliptical hot particle will not sediments in cold fluids when $Ar < 17$, as denoted by the green cross in Fig. 16. In cold fluids, the hot particle transfer heat to the surrounding fluids and causes natural convection in the direction opposite to the particle sediments direction; when the particle Archimedes number is small (i.e., the particle density is small), the upward buoyancy force may overcome downward gravity force on the particle thus hindering the particle sedimentation. As indicated in Fig. 17b, the forced

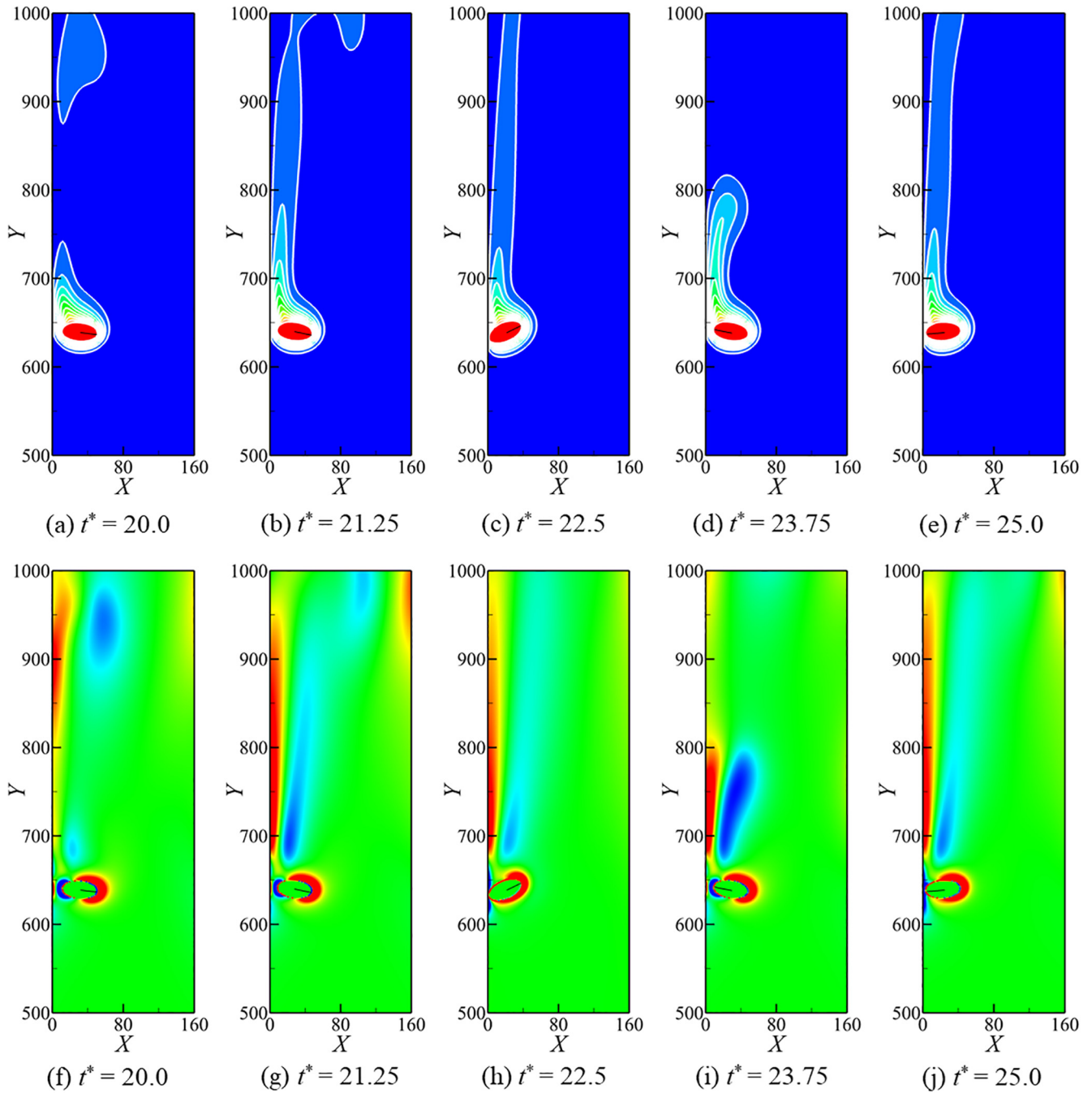


Fig. 19. Temperature and vorticity contours of the hot elliptical particle settling in a wide channel ($Ar = 26.19$, $Gr = 400$).

convection may even be neglected in the regimes when $Gr/Re_p^2 \gg 1$ (corresponding to low Ar and high Gr regime in Fig. 17a).

Compared to the sedimentation modes reported by Xia et al. [2] for an isothermal elliptical particle sediment within a wide channel, two new sedimentation modes are found due to thermal effects, namely the inclined mode and the anomalous rolling mode. Because we have discussed the horizontal mode, the horizontal II mode and the inclined mode for a cold elliptical particle sedimentation, in the following, we will only analyze the anomalous rolling mode. Fig. 18 shows typical trajectories and orientations of the particle when sediments in the anomalous rolling mode. The particle trajectory oscillates offsets the channel centerline (near the left wall), and the angle between particle major axis and horizontal direction changes periodically from 0 to 2π . The falling particle

rotates counterclockwise as if it was contacting and rolling up along the left channel wall, for this reason, the sedimentation mode is termed as "anomalous" rolling mode. The temperature contours and vorticity contours of the settling particle during a rolling period is visualized in Fig. 19a–e and f–j, respectively. It is also worth mentioning the anomalous rolling mode reported here is the result of combined wall effects and competition between natural and forced convection; while the inclined mode observed by Xia et al. [2] is merely the result of channel wall confinement. Here, the anomalous mode is bounded between the horizontal mode and inclined mode. For colder particle, the forced convection will be dominated and the particle sediments in the horizontal mode; for hotter particle, the natural convection will be dominated and the particle sediments in the inclined mode.

5. Conclusion

The sedimentation behavior of an elliptical thermal particle in the channel has been studied numerically. The phase diagram of the flow regimes as functions of Archimedes and Grashof numbers are obtained. From the phase diagram, it is observed that three new sedimentation modes appeared in the region with small Archimedes number where natural convection dominates. For the cold particle settling in a hot fluid, the tumbling mode and the inclined mode are identified; for the hot particle settling in a cold fluid, the anomalous rolling mode and the inclined mode are identified. These sedimentation modes are the results of channel wall confinement, combined forced and natural convection.

Conflict of interest

Authors declare that there is no conflicts of interest.

Acknowledgement

The work described in this paper was fully supported by a grant from the Research Grant Council of the Hong Kong Special Administrative Region, China (Project No. T23-601/17-R).

Appendix A. Supplementary material

Supplementary data associated with this article can be found, in the online version, at <https://doi.org/10.1016/j.ijheatmasstransfer.2018.05.073>.

References

- [1] A. Xu, W. Shyy, T. Zhao, Lattice Boltzmann modeling of transport phenomena in fuel cells and flow batteries, *Acta. Mech. Sin.* 33 (3) (2017) 555–574, <https://doi.org/10.1007/s10409-017-0667-6>.
- [2] Z. Xia, K.W. Connington, S. Rapaka, P. Yue, J.J. Feng, S. Chen, Flow patterns in the sedimentation of an elliptical particle, *J. Fluid Mech.* 625 (2009) 249–272, <https://doi.org/10.1017/S0022112008005521>.
- [3] T. Swaminathan, K. Mukundakrishnan, H.H. Hu, Sedimentation of an ellipsoid inside an infinitely long tube at low and intermediate Reynolds numbers, *J. Fluid Mech.* 551 (2006) 357–385, <https://doi.org/10.1017/S0022112005008402>.
- [4] H. Huang, X. Yang, X.-Y. Lu, Sedimentation of an ellipsoidal particle in narrow tubes, *Phys. Fluids* 26 (5) (2014) 053302, <https://doi.org/10.1063/1.4874606>.
- [5] X. Yang, H. Huang, X. Lu, Sedimentation of an oblate ellipsoid in narrow tubes, *Phys. Rev. E* 92 (6) (2015) 063009, <https://doi.org/10.1103/PhysRevE.92.063009>.
- [6] H. Gan, J. Chang, J.J. Feng, H.H. Hu, Direct numerical simulation of the sedimentation of solid particles with thermal convection, *J. Fluid Mech.* 481 (2003) 385–411, <https://doi.org/10.1017/S0022112003003938>.
- [7] Z.-G. Feng, E.E. Michaelides, Heat transfer in particulate flows with Direct Numerical Simulation (DNS), *Int. J. Heat Mass Transf.* 52 (3–4) (2009) 777–786, <https://doi.org/10.1016/j.ijheatmasstransfer.2008.07.023>.
- [8] N.G. Deen, S.H. Kriebitzsch, M.A. van der Hoef, J. Kuipers, Direct numerical simulation of flow and heat transfer in dense fluid-particle systems, *Chem. Eng. Sci.* 81 (2012) 329–344, <https://doi.org/10.1016/j.ces.2012.06.055>.
- [9] J. Hu, Z. Guo, A numerical study on the migration of a neutrally buoyant particle in a Poiseuille flow with thermal convection, *Int. J. Heat Mass Transf.* 108 (2017) 2158–2168, <https://doi.org/10.1016/j.ijheatmasstransfer.2017.01.077>.
- [10] B.-F. Wang, D.-J. Ma, C. Chen, D.-J. Sun, Linear stability analysis of cylindrical Rayleigh-Bénard convection, *J. Fluid Mech.* 711 (2012) 27–39, <https://doi.org/10.1017/jfm.2012.360>.
- [11] S.-N. Xia, Z.-H. Wan, S. Liu, Q. Wang, D.-J. Sun, Flow reversals in Rayleigh-Bénard convection with non-Oberbeck-Boussinesq effects, *J. Fluid Mech.* 798 (2016) 628–642, <https://doi.org/10.1017/jfm.2016.338>.
- [12] L. Fei, K.H. Luo, C. Lin, Q. Li, Modeling incompressible thermal flows using a central-moments-based lattice Boltzmann method, *Int. J. Heat Mass Transf.* 120 (2018) 624–634, <https://doi.org/10.1016/j.ijheatmasstransfer.2017.12.052>.
- [13] L. Fei, K.H. Luo, Cascaded lattice Boltzmann method for incompressible thermal flows with heat sources and general thermal boundary conditions, *Comput. Fluids* 165 (2018) 89–95, <https://doi.org/10.1016/j.compfluid.2018.01.020>.
- [14] P. Cheng, X. Quan, S. Gong, X. Liu, L. Yang, Recent analytical and numerical studies on phase-change heat transfer, *Adv. Heat Transf.* 46 (2014) 187–248, <https://doi.org/10.1016/bs.aiht.2014.08.004>.
- [15] Q. Li, K. Luo, Q. Kang, Y. He, Q. Chen, Q. Liu, Lattice Boltzmann methods for multiphase flow and phase-change heat transfer, *Prog. Energy Combust. Sci.* 52 (2016) 62–105, <https://doi.org/10.1016/j.pecs.2015.10.001>.
- [16] A. Xu, L. Shi, T. Zhao, Accelerated lattice Boltzmann simulation using GPU and OpenACC with data management, *Int. J. Heat Mass Transf.* 109 (2017) 577–588, <https://doi.org/10.1016/j.ijheatmasstransfer.2017.02.032>.
- [17] Z. Guo, C. Zheng, B. Shi, Discrete lattice effects on the forcing term in the lattice Boltzmann method, *Phys. Rev. E* 65 (4) (2002) 046308, <https://doi.org/10.1103/PhysRevE.65.046308>.
- [18] Z. Guo, C. Zheng, Analysis of lattice Boltzmann equation for microscale gas flows: relaxation times, boundary conditions and the Knudsen layer, *Int. J. Comput. Fluid Dyn.* 22 (7) (2008) 465–473, <https://doi.org/10.1080/10618560802253100>.
- [19] P. Lallemand, L.-S. Luo, Theory of the lattice Boltzmann method: Dispersion, dissipation, isotropy, Galilean invariance, and stability, *Phys. Rev. E* 61 (6) (2000) 6546, <https://doi.org/10.1103/PhysRevE.61.6546>.
- [20] J. Wang, D. Wang, P. Lallemand, L.-S. Luo, Lattice Boltzmann simulations of thermal convective flows in two dimensions, *Comput. Math. Appl.* 65 (2) (2013) 262–286, <https://doi.org/10.1016/j.camwa.2012.07.001>.
- [21] H. Huang, X. Yang, M. Krafczyk, X.-Y. Lu, Rotation of spheroidal particles in Couette flows, *J. Fluid Mech.* 692 (2012) 369–394, <https://doi.org/10.1017/jfm.2011.519>.
- [22] H. Huang, X.-Y. Lu, An ellipsoidal particle in tube Poiseuille flow, *J. Fluid Mech.* 822 (2017) 664–688, <https://doi.org/10.1017/jfm.2017.298>.
- [23] A. Xu, T. Zhao, L. Shi, X. Yan, Three-dimensional lattice Boltzmann simulation of suspensions containing both micro- and nanoparticles, *Int. J. Heat Fluid Flow* 62 (2016) 560–567, <https://doi.org/10.1016/j.ijheatfluidflow.2016.08.001>.
- [24] A. Xu, L. Shi, T. Zhao, Lattice Boltzmann simulation of shear viscosity of suspensions containing porous particles, *Int. J. Heat Mass Transf.* 116 (2018) 969–976, <https://doi.org/10.1016/j.ijheatmasstransfer.2017.09.060>.
- [25] M. Bouzidi, M. Firdauss, P. Lallemand, Momentum transfer of a Boltzmann-lattice fluid with boundaries, *Phys. Fluids* 13 (11) (2001) 3452–3459, <https://doi.org/10.1063/1.1399290>.
- [26] P. Lallemand, L.-S. Luo, Lattice Boltzmann method for moving boundaries, *J. Comput. Phys.* 184 (2) (2003) 406–421, [https://doi.org/10.1016/S0021-9991\(02\)00022-0](https://doi.org/10.1016/S0021-9991(02)00022-0).
- [27] R. Mei, L.-S. Luo, W. Shyy, An accurate curved boundary treatment in the lattice Boltzmann method, *J. Comput. Phys.* 155 (2) (1999) 307–330, <https://doi.org/10.1006/jcph.1999.6334>.
- [28] R. Mei, W. Shyy, D. Yu, L.-S. Luo, Lattice Boltzmann method for 3-D flows with curved boundary, *J. Comput. Phys.* 161 (2) (2000) 680–699, <https://doi.org/10.1006/jcph.2000.6522>.
- [29] D. Yu, R. Mei, L.-S. Luo, W. Shyy, Viscous flow computations with the method of lattice Boltzmann equation, *Prog. Aerosp. Sci.* 39 (5) (2003) 329–367, [https://doi.org/10.1016/S0376-0421\(03\)0003-4](https://doi.org/10.1016/S0376-0421(03)0003-4).
- [30] B. Chun, A. Ladd, Interpolated boundary condition for lattice Boltzmann simulations of flows in narrow gaps, *Phys. Rev. E* 75 (6) (2007) 066705, <https://doi.org/10.1103/PhysRevE.75.066705>.
- [31] L. Li, R. Mei, J.F. Klausner, Boundary conditions for thermal lattice Boltzmann equation method, *J. Comput. Phys.* 237 (2013) 366–395, <https://doi.org/10.1016/j.jcp.2012.11.027>.
- [32] L. Li, R. Mei, J.F. Klausner, Lattice Boltzmann models for the convection-diffusion equation: D2Q5 vs D2Q9, *Int. J. Heat Mass Transf.* 108 (2017) 41–62, <https://doi.org/10.1016/j.ijheatmasstransfer.2016.11.092>.
- [33] A.J. Ladd, Numerical simulations of particulate suspensions via a discretized Boltzmann equation. Part 1. Theoretical foundation, *J. Fluid Mech.* 271 (1) (1994) 285–309, <https://doi.org/10.1017/S0022112094001771>.
- [34] B. Wen, C. Zhang, Y. Tu, C. Wang, H. Fang, Galilean invariant fluid-solid interfacial dynamics in lattice Boltzmann simulations, *J. Comput. Phys.* 266 (2014) 161–170, <https://doi.org/10.1016/j.jcp.2014.02.018>.
- [35] Z.-G. Feng, E.E. Michaelides, The immersed boundary-lattice Boltzmann method for solving fluid-particles interaction problems, *J. Comput. Phys.* 195 (2) (2004) 602–628, <https://doi.org/10.1016/j.jcp.2003.10.013>.
- [36] C.K. Aidun, Y. Lu, E.-J. Ding, Direct analysis of particulate suspensions with inertia using the discrete Boltzmann equation, *J. Fluid Mech.* 373 (1998) 287–311, <https://doi.org/10.1017/S0022112098002493>.
- [37] Z. Yu, X. Shao, A. Wachs, A fictitious domain method for particulate flows with heat transfer, *J. Comput. Phys.* 217 (2) (2006) 424–452, <https://doi.org/10.1016/j.jcp.2006.01.016>.
- [38] S.K. Kang, Y.A. Hassan, A direct-forcing immersed boundary method for the thermal lattice Boltzmann method, *Comput. Fluids* 49 (1) (2011) 36–45, <https://doi.org/10.1016/j.compfluid.2011.04.016>.